Contents list available at IJRED website

International Journal of Renewable Energy Development

Journal homepage: https://ijred.undip.ac.id

Research Article

Three-dimensional CFD-solid mechanics analysis of the hydrogen internal combustion engine piston subjected to thermomechanical loads

Maher A.R. Sadiq Al-Baghdadi, Sahib Shihab Ahmed, Nabeel Abdulhadi Ghyadh*

Department of Mechanical Engineering, Faculty of Engineering, University of Kufa, Iraq

Abstract. Fueling internal combustion engines with hydrogen is one of the most recommended alternative fuels today in order to combat the energy crisis, pollution problems, and climate change. Despite all the advantages of hydrogen fuel, it produces a higher combustion temperature than gasoline. In an internal combustion engine, the piston is among the numerous complex and highly loaded components. Piston surfaces are directly affected by combustion flames, making them critical components of engines. To examine the stress distribution and specify the critical fracture zones in the piston for hydrogen fuel engines, a three-dimensional CFD-solid-mechanics model of the internal combustion engine piston subjected to real thermomechanical loads was analyzed numerically to investigate the distribution of the temperature on the piston body, the interrelated thermomechanical deformations map, and the pattern of the stresses when fueling the engine with hydrogen fuel. With the aid of multiphysics COMSOL software, the CFD-solid-mechanics equations were solved with high accuracy. Despite the increase in pressure on the piston and its temperature when the engine is running on hydrogen fuel, the results show that the hydrogen fuel engine piston can withstand, safely, the thermomechanical loads. In comparison to gasoline fuel, hydrogen fuel caused a deformation of 0.34 mm, an increase of 17%. This deformation is within safe limits, with an average clearance of 0.867 mm between the cylinder liner and piston.

Keywords: Hydrogen fuel; Internal combustion engines; Piston; Thermomechanical loads; Computational Fluid Dynamics (CFD).

Received: 15th January 2023; Revised: 28th March 2023; Accepted: 7th April 2023; Available online: 25th April 2023

1. Introduction

Carbon oxides, nitrogen oxides, hydrocarbons, soot, sulfur oxides, and a variety of volatile organic compounds are among the most common emissions from internal combustion engines fueled by fossil fuels. Research has focused on the fuels economy by adopting strategies of reducing fuel consumption and environmental impact by lowering the toxic component concentration in combustion products through the use of alternative fuels in response to today's energy crisis, pollution problems, and climate change (Pingkuo and Han, 2022). Hydrogen is considered an ideal alternative fuel. Compared to other chemical fuels, hydrogen burns cleanest (Scovell, 2022). Hydrogen fuel has the potential to play a role in reducing greenhouse gas emissions and combating climate change. When produced using renewable energy sources, hydrogen can be a clean and emission-free fuel for transportation, heating and power generation. Using non-fossil energy, it can be produced from water and the combustion process returns water to its original state (Ikonnikova *et al.*, 2022). Hydrogen ignites with a smaller amount of energy than gasoline. With hydrogen engines, lean mixtures can be ignited quickly due to the lower ignition energy of hydrogen fuel (Ikonnikova *et al.*, 2022; Vichos *et al.*, 2022). One of the most stressed parts of an internal combustion engine is its piston (Ismail *et al.*, 2020; Mancaruso and Sequino, 2019). In addition to being subjected to an excessive amount of thermal stress, the piston in the combustion chamber is exposed to large axial and lateral loads as well as inertia forces during the power cycles (Najafi *et al.*, 2019; Garbinčius *et al.*, 2005). In order to avoid any failure of the piston body, it is important to study the combined thermal and mechanical forces acting on it, especially when using alternative fuel for the engine or introducing a new design (Durat *et al.*, 2022; Tan *et al.*, 2022).

To understand the deformed shape of the engine piston and its strength, computerized finite volume analysis techniques were used since they simulate and calculate combined thermal loads due to high gas temperatures and mechanical loads due to high gas pressures on the piston (Ismail *et al.*, 2020; Najafi *et al.*, 2019).

Under all operating conditions, particularly when there is a large amount of power being output, the piston of the internal combustion engine should possess high strength. Using a numerical model, Ismail *et al.*, (2020) studied the effect on piston loading by increasing the boosting pressure until achieving the maximum engine power possible by analyzing the thermomechanical loads on the whole body of the piston. According to their results, the piston is in a safe condition and can withstand additional stress loads up to the additional power that can reach 56%.

* Corresponding author
Email: nabeel.ghayadh@uokufa.edu.iq (N.A. Ghyadh)

https://doi.org/10.14710/ijred.2023.52496
ISSN: 2252-4940/© 2023.The Author(s). Published by CBIORE

A major issue in improving combustion engine efficiency is heat losses. Moreover, engine components such as pistons, as well as their thermal state, need to be considered. Mancaruso and Sequino, (2019) measured experimentally the piston temperature of the internal combustion engine during operation to evaluate heat losses and engine efficiency. Their study provided them with experimental data that enabled them to build a one-dimensional model of heat transfer using only theoretical data.

Since redesigning and manufacturing a new engine would be very expensive, engineers evaluate the consequences of upgrading an already-designed engine to get higher performance. An increase in engine power was achieved by increasing engine speed and combustion gas pressure (Najafi *et al.*, 2019). The life of a piston decreases by 4000 times when engine power increases to reach the maximum stress of 50%. Lower ring grooves and pinholes are critical areas for engine pistons when power increases (Najafi *et al.*, 2019).

Using the influence of changes in heat transfer conditions and scale deposits on the outer surface of cylinders, Garbinčius *et al.*, (2005) investigated numerically the variation of thermal gaps between pistons and cylinders. Compared with the case without scale deposits, their results showed a 0.02 mm increase in piston deformations and a 0.025 mm increase in cylinder deformations.

Many studies have examined the effects of thermal barrier coatings on the pistons of internal combustion engines, particularly how it reduces the amount of heat that is rejected from the cylinder in adiabatic engines (Durat *et al.*, 2012; Tan *et al.*, 2022; Zhou *et al.*, 2022). The combustion process and exhaust emission characteristics are, however, affected by the insulation of the engine piston. Insulation of the engine's pistons can reduce the heat transfer between the gases in the cylinder and the piston wall and thus increase the combustion temperature inside the cylinder (Durat *et al.*, 2012; Tan *et al.*, 2022).

In an engine, the piston plays a crucial role due to its direct contact with combustion flames (Deulgaonkar *et al.*, 2021). Microstructure plays a significant role in most piston failures (Satyanarayana *et al.*, 2018; Lohakare *et al.*, 2022). Cracks are usually the cause of failure in the pinhole or skirt of the piston (Venkatachalam and Kumaravel, 2019; Zhenwei *et al.*, 2022).

Temperature distributions are crucial for engine piston life and durability (Koutsakis *et al.*, 2022; Azadi and Parast, 2022). It is very important to determine the temperature distributions with high accuracy in order to determine the thermal stress distribution and critical fracture zones in the engine piston (Dudareva *et al.*, 2017; Kakaee *et al.*, 2015; Gai and Zhao, 2022). However, investigating with high accuracy the temperature distribution on the engine piston body and the thermomechanical deformations resulting from fueling the internal combustion engine with hydrogen fuel is still lacking. This work aims to cover this shortcoming using a three-dimensional computational fluid dynamics (CFD) solid mechanics model subjected to actual thermomechanical loads to examine the stress distribution and specify the critical fracture zones in the piston for hydrogen fuel engines.

2. Methodology

Several steps are involved in the modelling process. Modelling begins with the computational domain of a piston engine. COMSOL's library and its CAD tools have been used to construct a geometry model of the engine piston in three dimensions. An analysis of heat transfer processes within the combustion chamber is included in the thermal modelling process to determine the temperature distribution inside the piston. The solid mechanics model has been applied to determine the mechanical as well as thermal stresses inside the piston body, in addition to the total deformation. A thermodynamic engine power cycle simulation model has been employed to calculate the pressure and temperature inside the combustion chamber. The finite volume model of the CFD-solid mechanics applies mechanical and thermal boundary conditions simultaneously. The final step is to generate the mesh and solve the governing equations for the model. These steps are detailed in the following subsections.

2.1. CFD thermal model

An internal combustion engine piston 3D model based on the finite volume method (FVM) is presented. In this model, the engine piston is subject to mechanical and thermal loads arising during its operation. The computational domain in the whole three dimensions of the geometry of the engine piston sitting on the connecting road is shown in Figure 1.

Heat transfer equations related to conduction and convection, as well as the appropriate boundary conditions, are used to predict the map of the temperatures within the engine pistons.

In the piston of the internal combustion engine, the heat transfer takes place is governed by the following equation (Cerit and Coban, 2014; Cerit, 2011);

$$\rho c_p \frac{\partial T}{\partial t} + \rho c_p \mathbf{u}.\nabla T = \nabla.(k\nabla T) + Q \quad (1)$$

where Q is the source of the heat from the combustion of the fuel [W], $\mathbf{u}$ denotes the velocity vector [m/s], t refers to time [s], c_p is referring to the piston material heat capacity [kJ/kg.K], ρ is denoting to the piston material density [kg/m^3], T denotes the temperature [K], and k is referring to the piston material thermal conductivity [W/m.K].

2.2. Solid mechanics model

The following equations will be used to determine the mechanical as well as thermal stresses inside the piston body of

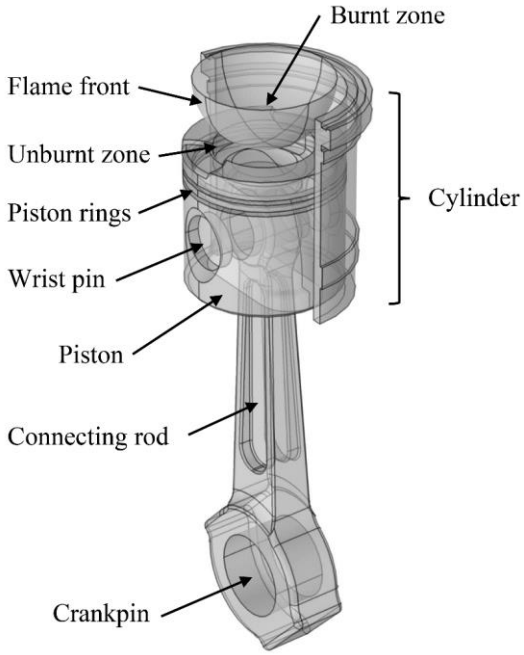

Fig 1. The geometry domain of a piston assembly in an engine.

Table 1
Piston and ring thermomechanical properties.

Property	Rings	Base metal (AlSi piston)
Young's modulus [GPa]	200	69
Poisson's ratio	0.3	0.33
Thermal conductivity [W/m °C]	16	155
Thermal expansion 10^{-6} [1/°C]	10	21
Density [Kg/m^3]	7300	2700
Specific heat [J/kg °C]	460	960

the internal combustion engine (Cerit and Coban, 2014; Cerit, 2011);

$$-\nabla.\sigma = \mathbf{F}\epsilon \tag{2}$$

where σ is the stress [Pa], F is the constitutive matrix, and ϵ refers to strains.

Changing the temperature of an unconstrained isotropic volume results in thermal strains, which can be calculated as follows (Cerit and Coban, 2014; Cerit, 2011);

$$\epsilon_{th} = \alpha\left(T - T_{ref}\right) \tag{3}$$

where T_{ref} is the piston reference temperature and α refers to the thermal expansion of the piston material [1/K].

The thermomechanical properties of the piston with the rings of the internal combustion engine are summarized in Table 3 (Cerit and Coban, 2014).

2.3. Thermodynamic engine cycle model

During the combustion process of an engine, the piston is subjected to heat fluxes and pressure forces caused by hot gases. To predict the pressure and temperature inside the combustion chamber, the power cycle has been simulated with high accuracy by two zones internal combustion engine model. The model predicts mass burning rates, heat release rates, accumulated heat releases, the composition of burned and unburned zones, the temperature of burned and unburned zones, cylinder pressure, the loss of heat by radiation and convection, the energy loss resulting from flow into crevices, the concentration of pollutants emitted, and the performance of the engine.

Using the two zones model, the internal combustion engine combustion chamber has been generally divided into burned (reaction) and unburned (premixed) zones separated by a flame front (Figure 1). Combustion products are assumed to remain within the reaction zone where the chemical reaction occurs. The unburned zone is filled with a premixed gas mixture. The process of modelling includes taking into account both the thermodynamic properties of the mixture and the individual chemical species in the two zones. A thermodynamic analysis of the burned and unburned zones was conducted in accordance with the first law of thermodynamics, equation of state, and conservations of mass and volume. Throughout the cylinder charge, it was assumed that the pressure would be uniform.

The two zones simulation model that was used in the present work is an extension of the work of Al-Baghdadi and Al-Janabi (1999, 2000, 2003). In addition, the model has been extensively enhanced and developed in order to accommodate a wide variety of different engine models that are working with different types of fuels (Al-Baghdadi, 2000, 2004, 2005, 2006).

The following equation was used to model the mass burning rate;

$$\frac{dM_b}{dt} = A_{fl}.\rho.ST \tag{4}$$

In the mass burning rate equation, the A_{fl} denotes the area of the flame front [m^2], ρ refers to the density of the gas mixture [kg/m^3], and ST refers to the turbulent flame front speed [m/s].

The following equation can be used to calculate the heat transfer coefficient at the piston head of the internal combustion engine (Cerit and Coban, 2014);

$$h_g(\theta) = 3.26\left(P_g(\theta)\right)^{0.8}\left(6.18 \times V_p\right)^{0.8}\left(b^{-0.2}\right)\left(T_g(\theta)\right)^{-0.55} \tag{5}$$

where θ is the crankshaft angle [degree], P_g refers to the gas pressure inside the cylinder [Pa], V_p denotes the mean engine piston speed during the power cycle [m/s], b denotes the engine piston bore dimension [mm], T_g refers to the gas temperature inside the combustion chamber [K], and h_g denotes the heat transfer coefficient at the piston head [W/m^2.K].

The resulting gas temperature (T_{gr}) and mean heat transfer coefficient (h_{gm}) can be calculated as follows because of the high gases temperature as well as pressure variations inside the combustion cylinder during the engine power cycle (Cerit and Coban, 2014);

$$T_{gr} = \frac{\left(h_g T_g\right)_m}{h_{gm}} \tag{6}$$

$$h_{gm} = \frac{1}{720}\int_0^{720} h_g(\theta)d\,\theta \tag{7}$$

$$\left(h_g T_g\right)_m = \frac{1}{720}\int_0^{720} h_g(\theta)T_g(\theta)d\theta \tag{8}$$

An overview of the combustion engine specifications and the operating conditions are provided in Table 2 (Al-Baghdadi and Al-Janabi, 1999; Al-Baghdadi, 2000). Hydrogen and gasoline fuel properties are listed in Table 3 (Al-Baghdadi and Al-Janabi, 1999; Al-Baghdadi, 2006).

Table 2
Conditions of operation and specifications of the engine.

Engine specification	
Dimension of the piston bore [mm]	80
Dimension of the connecting rod [mm]	200
Number of the cylinders	4
Compression ratio	7.5
Engine speed [rpm]	1500
Equivalence ratio	1

Table 3
Properties of hydrogen and gasoline fuels.

Property	Hydrogen	Gasoline
Chemical formula	H_2	C_8H_{18}
Molar carbon to hydrogen ratio	0.0	0.444
Stoichiometric air/fuel ratio, mass	34.32	15.11
Combustion speed in air (m/s)	2.65 - 3.25	0.37 - 0.43
Lower heating value (MJ/kg)	119.93	44.5
Flammability limits (% by volume)	4.1 - 74	1.2 - 6
Working mixture equivalence ratio Ø	0.1 - 7.1	0.6 - 3.5
Minimum ignition energy in the air [mJ]	0.02	0.24
Self-ignition temperature (K)	855	530
Octane number	130+	86-94

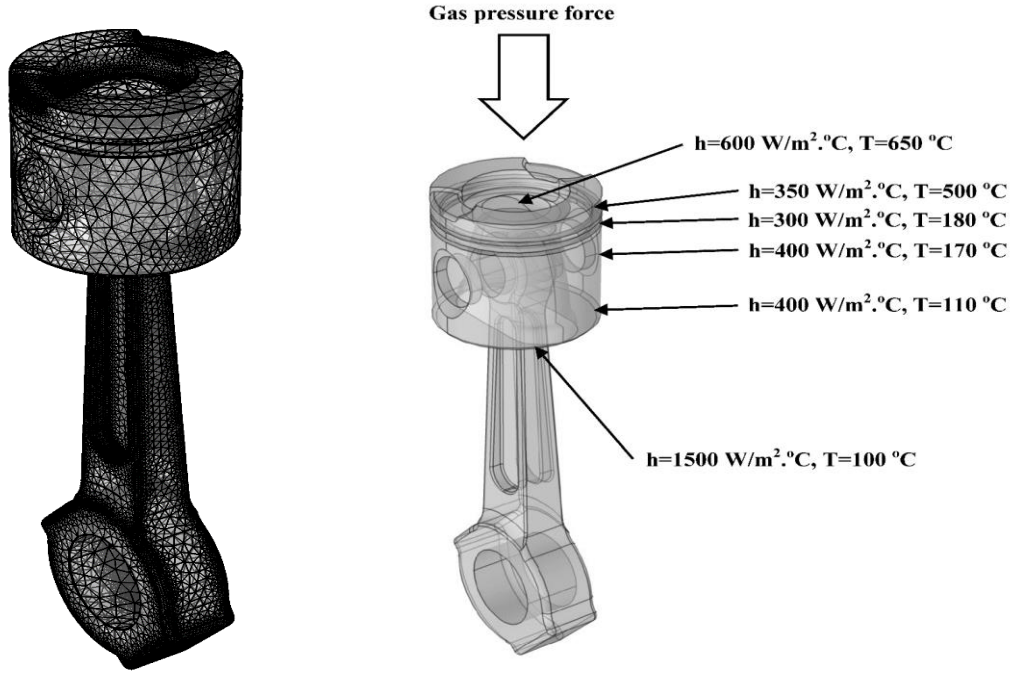

Fig 2. Computational mesh (a) and boundary conditions (b).

2.4. Modelling parameters

Finite-volume methods were used to discretize the equations and multiphysics COMSOL software was used to solve them. An accurate grid is found by adopting a fine quadratic mesh and finding the minimum number of cells. The numerical tests were performed in accordance with stringent numerical standards to ensure that their results were independent of grid size. In order to obtain a satisfactory spatial resolution, a quadratic mesh consisting of 203143 elements of the domain part, 43024 elements of the boundary parts, and 6392 elements of the edge parts was seen to be adequate (Figure 2a). Furthermore, mechanical boundary conditions were applied along with the heat transfer boundary conditions (Figure 2b). During the power cycle, the engine piston surface is exposed to a large amount of heat and pressure resulting from the combustion process. Based on the results of the thermodynamic engine cycle model simulation, the mean piston temperature and the mean heat transfer coefficient have been calculated and used as thermal boundary conditions. As a mechanical boundary condition, the upper surface of the piston engine has been considered as the area where the gas pressure inside the cylinder acts upon. In an iterative solution, the relative error in each field between consecutive iterations was less than 1.0×10^{-6}, indicating that the solution was convergent.

3. Results and discussions

3.1. Thermodynamic power cycle

In addition to the heat flux caused by the combustion of the fuel, the piston of the engine is also exposed to the hot gas pressure forces within the combustion chamber (Nguyen-Thi, T. X., and Bui, 2023; Ramegouda and Joseph, 2021). As a function of the crankshaft angle, the cylinder pressure inside the combustion chamber and the temperature of each burned and unburned zone for the power cycle are shown for each case of the gasoline-fueled engine and hydrogen-fueled engine (Figures 3). In the hydrogen fuel engine, there is a clear increase in the peak gas pressure inside the cylinder and peak burned and unburned temperatures. The high hydrogen combustion

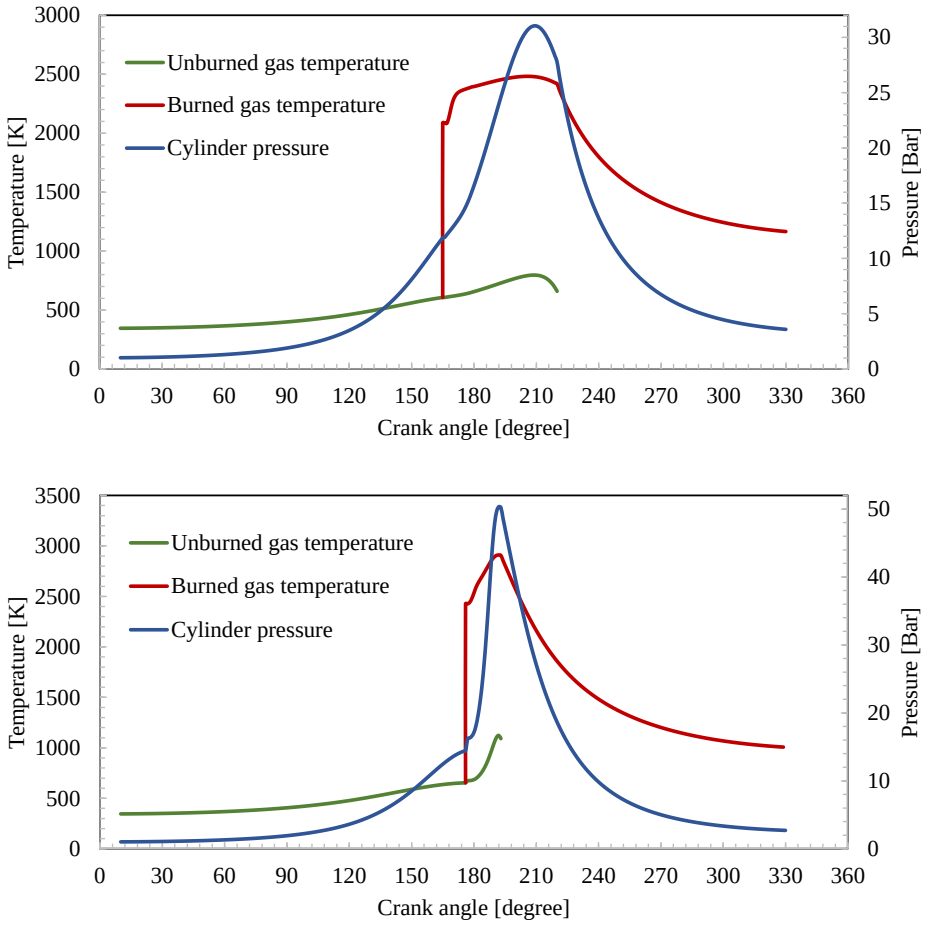

Fig 3. An analysis of the variation in-cylinder pressure, unburned and burned temperatures as a function of crank angle: (a). gasoline fuel and (b). hydrogen fuel.

expansion rates increase the cylinder pressure. Furthermore, the gas pressure diagram inside the cylinder approaches closer to the ideal cycle diagram, where the period of the combustion process decreases. The peak gas pressure increases from 31 bar to 50 bar, and the peak burned gas temperature increases from 2482.36 K to 2909.84 K. The reason for this is that the flam speed increases, and hence, mass burning of the fuel is increasing at a faster rate. As a result, the combustion process takes less time, which results in a reduction in heat transfer to cylinder walls, a reduction in exhaust gas temperature, a higher overall internal combustion engine efficiency, and a decrease in knocking.

3.2. Temperature distributions

As a result of the simulation model, Figures 4 and 5 show the temperature distributions at all points of the body of the assembly piston. There is an uneven distribution of steady-state

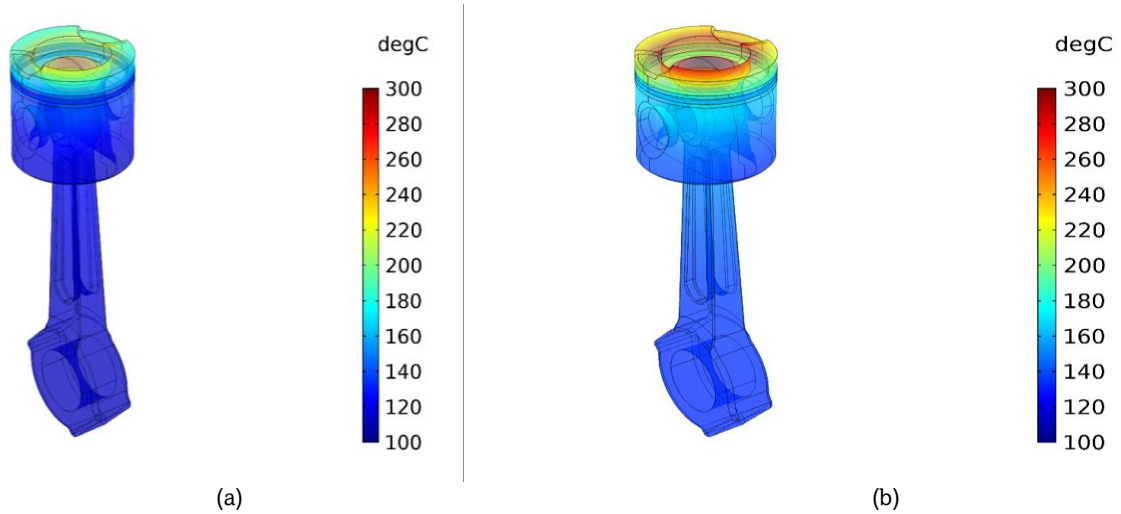

Fig 4. Temperature distribution along the overall assembly engine piston: (a). gasoline fuel and (b). hydrogen fuel.

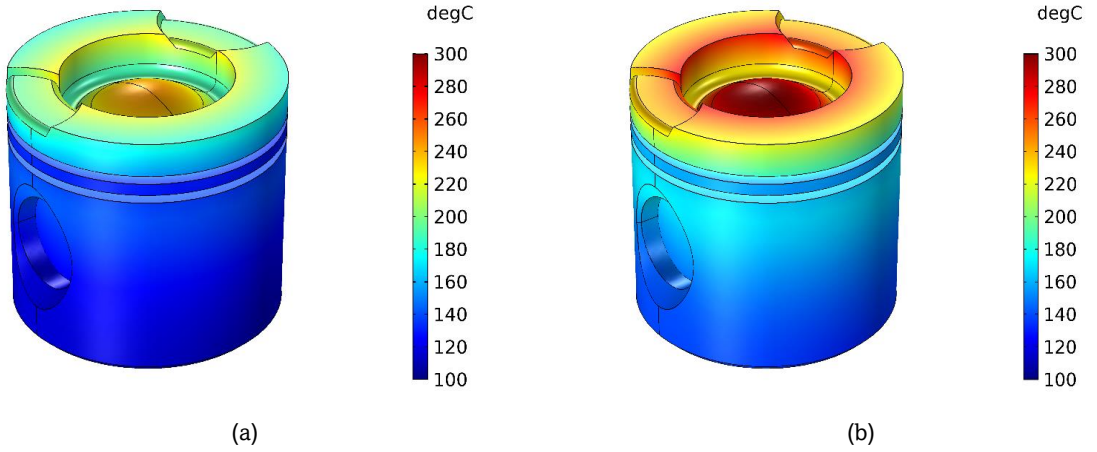

Fig 5. The temperatures map of the engine piston body for two case studies: (a). gasoline fuel and (b). hydrogen fuel.

temperatures across the piston crown edges and piston center, with the highest values occurring there. Piston temperatures for the gasoline fuel engine are 246.4°C, while piston temperatures for the hydrogen fuel engine are 300.8°C. For the gasoline fuel engine, the maximum temperature variation is from 161.7°C to 187.4°C at the groove of the first ring. The range of temperatures changed from 176.4°C to 195.2°C for the hydrogen fuel engine, which indicates a greater thermal load. Gasoline fuel engine piston skirt temperatures variation from 112.6°C to 130.8°C, while hydrogen fuel engine case temperatures range from 136.5°C to 167.4°C. Temperature distribution in the piston's significant vital region (the inner edge of pin bosses on the upper surface) within this range between 119°C and 146°C for the gasoline fuel engine case study. In comparison, the hydrogen engine case goes between 143°C and 177°C. The total mechanical and thermal stresses induced in these areas of the piston material remain in the elastic zone when temperature values reach this level, due to the material of

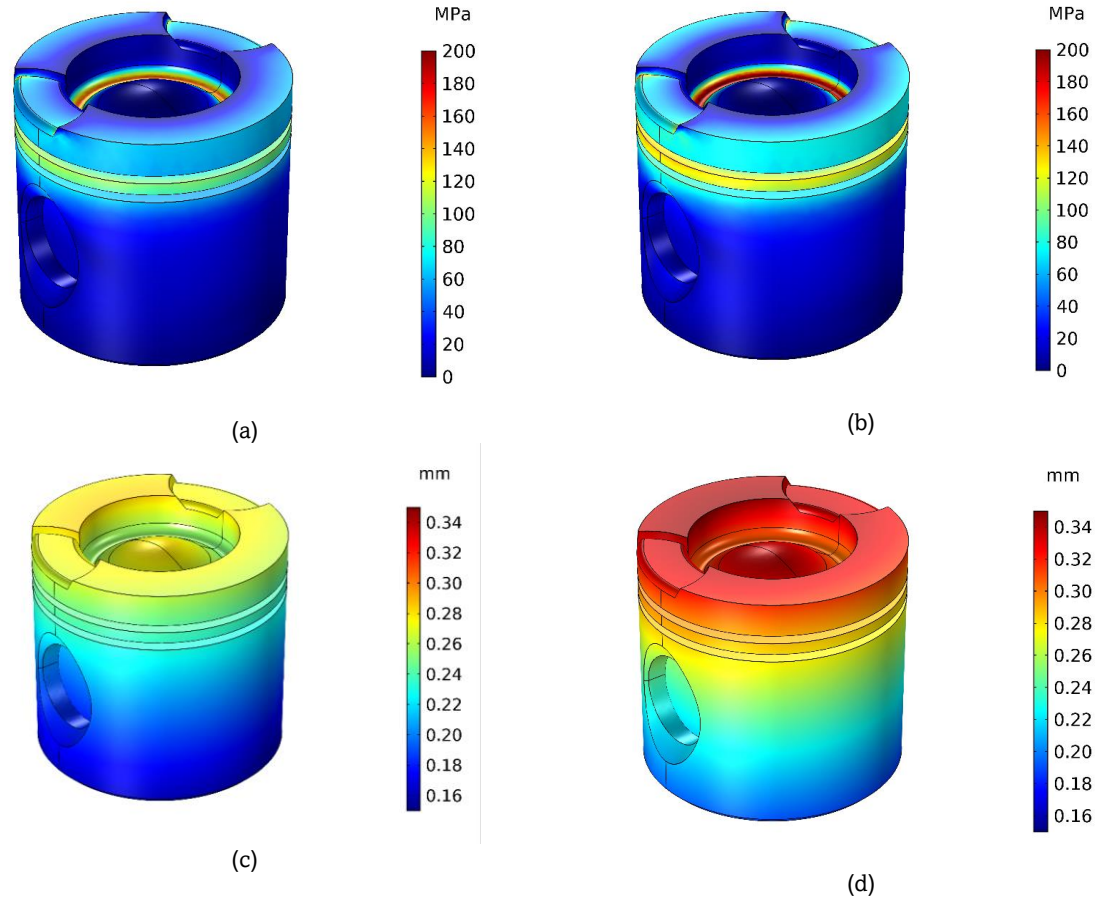

Fig 6. von Mises stresses distributions over the piston of the engine: (a). gasoline fuel and (b). hydrogen fuel; and piston engine deformation: (c). gasoline fuel and (d). hydrogen fuel.

the engine piston's yield limit value being high enough to provide sufficient strength.

3.3. Stresses and deformation distributions

Hydrogen combustion generates high temperatures, leading to thermal expansion and increased thermal stress on the piston body. Moreover, the high product gas pressure of hydrogen combustion creates high mechanical loading stress on the piston body. According to Figure 6a and Figure 6b, both thermal load and combustion pressure contributed to the stress map of the engine piston. In both the gasoline fuel case study and hydrogen fuel case study engines, the piston is subject to a maximum von Mises stress of 183.9 MPa and 221.8 MPa, respectively. Additionally, the inner surface edges for the pin bosses, and the upper and lower surfaces of the combustion bowl, are subjected to significant stress. Approximately 48.9 MPa of stress are measured at these regions in the case of the gasoline fuel engine and 58.9 MPa in the case of the hydrogen fuel engine. A combination of temperature differences between hot and cold regions and combustion gas pressure contributed to these stresses.

Mechanical and thermal loads are increased on the piston body during hydrogen combustion due to the high expansion rates and high flame temperatures. A representation of the engine piston deformation distributions under both the product of combustion gas pressure in addition to the gas high-temperature load are shown in Figure 6c and Figure 6d. It is important to note that the deformation of the piston is assessed based on the contact conditions between the assembled bodies analyzed as well as the imposed constraints. Radial and axial distributions of deformation are observed. According to the results, both temperature and pressure served as principal contributor piston's deformation. In the gasoline fuel engine case study, the maximum deformation suffered by the piston was 0.285 mm, and in the case of the hydrogen fuel engine, it was 0.346 mm. Piston crown edges, which are closest to hot gasses and to the coolant medium, are the most susceptible to this phenomenon. Additionally, the skirt's bottom area can be noted, the deformation of the piston decreases gradually, and it is still within a safe margin when it reaches the bottom. In the case of an engine operating under normal conditions, the safe margin is equal to 0.867mm which lies between the outer engine piston body and the inner cylinder liner.

3.4. Contact pressure distributions

Combustion gases exert force on the piston and connecting rods of an engine through piston pins. By swinging the connecting rod, it transfers reciprocating motions and combustion forces to the crankshaft by rotating the crank. Due to extreme operating temperatures, high combustion pressure, and high loads, piston pins must operate in severe conditions. High surface pressure at the contact regions between the assembled engine piston parts plays an important in piston failure (Kowalski *et al.*, 2023). As the piston is pushed against the pin boss due to the downward force acting on the piston, high pressure on the surface is created at the contact region of the

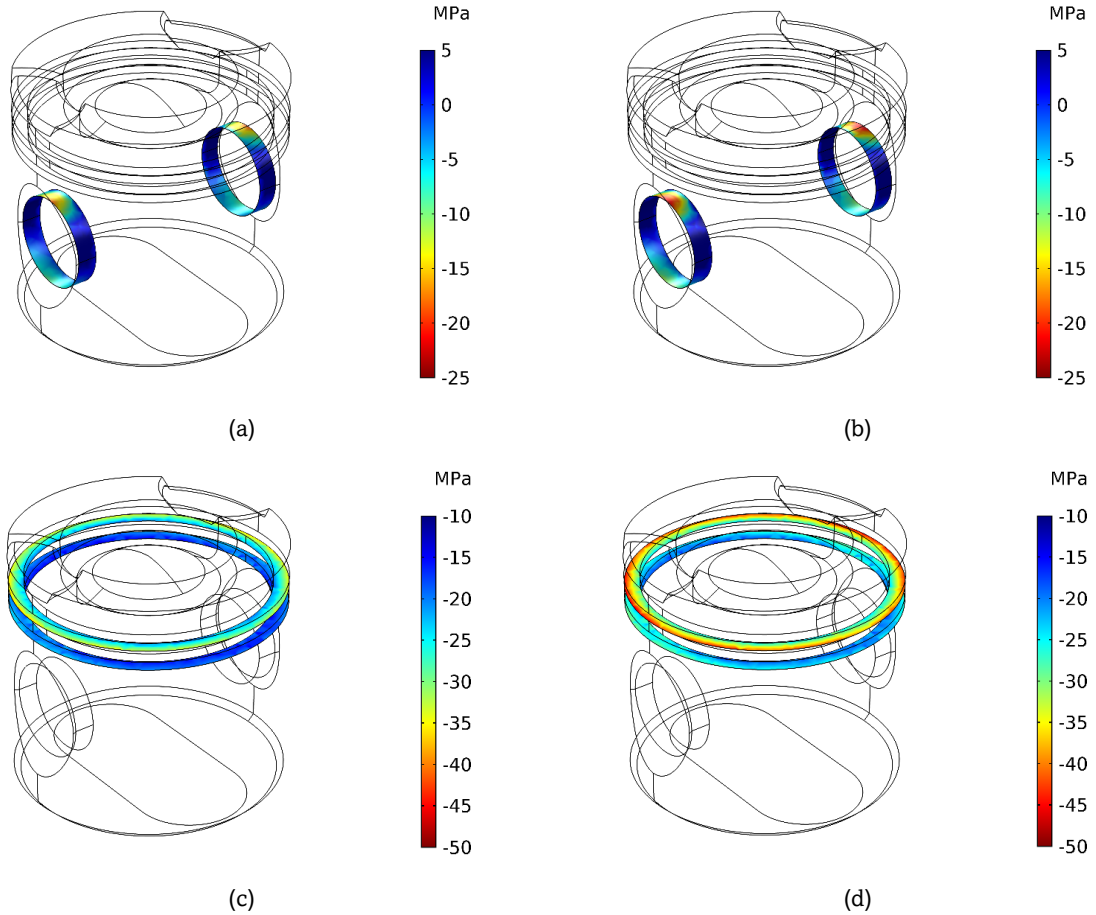

Fig 7. The distribution of the pressure over the piston pin bosses: (a). gasoline fuel and (b). hydrogen fuel; and over the piston compression rings: (c). gasoline fuel and (d). hydrogen fuel.

pin bosses. As shown in Figure 7a and Figure 7b, this pressure is usually found at the pin boss edges, with a maximum of 20.3 MPa for the gasoline fuel engine case study and 25.2 MPa for the hydrogen fuel engine case study. The assembly parts of the piston engine experience high-pressure loads in the case of hydrogen fuel due to hydrogen combustion's high expansion rates. A little bit more friction, heat generation, surface damage and noise perspective can be expected for the hydrogen fuel engine due to the asperity contact forces.

An important source of friction also occurs in the piston-ring-liner compartment. There is a circular distribution of pressure that occurs along the first landside of the piston compression rings, as shown in Figure 7c and Figure 7d. The maximum pressure value in the gasoline fuel engine case study is 37.8 MPa, while the maximum pressure in the hydrogen fuel engine case is 47.1 MPa, located at the first edges of the compression rings. Because hydrogen combustion's expansion rates are high, piston compression rings are subjected to high pressures in this case. Hydrogen fuels are therefore expected to generate slightly more heat as a result of piston compression ring friction.

Accordingly, from the results of the contact pressure in both piston pin bosses and piston compression rings, attention must be paid to the issue of good lubrication and the quality of the oil used in the case of engines that run on hydrogen fuel.

4. Conclusions

There has been an investigation of the mechanical loading in addition to the thermal loading of a piston body of an engine fueled by hydrogen fuel, and the results of this study have been presented. Throughout the study, an approach is introduced for simulating the real conditions of the piston contacting with other parts of the engine as well as the actual loading of the piston, constraints, and other factors in the engine. The study demonstrates the effect of temperature changes, stresses and deformations at points where the piston is most loaded, as well as the distribution of contact pressure. In general, the maximum temperature values are located on the edge of the top face of the piston, and they are identified from there. In the hydrogen fuel engine, the highest temperature is 300.8C. This is more than in a gasoline fuel engine by 18%. The highest stress is located at the edges of the bowl lip areas of the crown of the piston's top face. In the hydrogen fuel engine, the highest value of von Mises stress is 221.8 MPa. This is more than in a gasoline fuel engine by 17%. The highest deformation is located and indicated at the piston crown edges areas of the piston's highest face. In the hydrogen-fueled engine, the highest deformation is 0.346 mm. This is more than in a gasoline fuel engine by 17.6%. With an average clearance of 0.867 mm between the cylinder liner and piston, this deformation is within safe limits. Engine piston pin bosses have a high contact pressure on their upper inner surfaces. The highest value for the hydrogen fuel engine is 25.2 MPa. This is more than in a gasoline fuel engine by 19.4%. The highest pressure over the piston compression rings occurs along the first landside. There is maximum value that can be reached for the hydrogen fuel engine is 47.1 MPa. This is more than in a gasoline fuel engine by 19.7%.

Acknowledgements

A special thanks go to the Internal Combustion Engine laboratory at the department of Mechanical Engineering, Kufa University. Furthermore, Kufa Centre for Advanced Simulation in Engineering (KCASE) is highly regarded.

Author Contributions: Maher A.R. Sadiq Al-Baghdadi: Conceptualization, methodology, writing-original draft, supervision; Sahib Shihab Ahmed: Visualization, writing-review, and editing; Nabeel Abdulhadi Ghyadh: Resources, visualization, and editing. All authors have read and agreed to the published version of the manuscript.

Conflicts of Interest: The authors declare no conflict of interest.

References

Al-Baghdadi, M.A.R.S. (2000). Performance study of a four-stroke spark ignition engine working with both of hydrogen and ethyl alcohol as supplementary fuel. *International Journal of Hydrogen Energy* ,25(10), 1005-1009. https://doi.org/10.1016/S0360-3199(00)00012-4

Al-Baghdadi, M.A.R.S. (2004). Effect of compression ratio, equivalence ratio and engine speed on the performance and emission characteristics of a spark ignition engine using hydrogen as a fuel. *Renewable Energy*, 29(15),2245-2260. https://doi.org/10.1016/j.renene.2004.04.002

Al-Baghdadi, M.A.R.S. (2005). Development of a pre-ignition submodel for hydrogen engines. *Proceedings of the Institution of Mechanical Engineers, Part D: Journal of Automobile Engineering*. 29(10), 1203-1212. https://doi.org/10.1243/095440705X34883

Al-Baghdadi, M.A.R.S. (2006). A Simulation Model for a Single Cylinder Four-Stroke Spark Ignition Engine Fueled with Alternative Fuels, *Turkish Journal of Engineering and Environmental Sciences,* 30(6), 331-350. https://doi.org/10.3906/tar-1110-28

Al-Baghdadi, M.A.R.S., and Al-Janabi, H.A.K.S. (1999). A prediction study of the effect of hydrogen blending on the performance and pollutants emission of a four stroke spark ignition engine. *International Journal of Hydrogen Energy,* 24(4), 363-375. https://doi.org/10.1016/S0360-3199(98)00040-8

Al-Baghdadi, M.A.R.S., and Al-Janabi, H.A.K.S. (2000). Improvement of performance and reduction of pollutant emission of a four stroke spark ignition engine fueled with hydrogen–gasoline fuel mixture. *Energy Conversion and Management,* 41(1), 77-91. https://doi.org/10.1016/S0196-8904(99)00080-1 .

Al-Baghdadi, M.A.R. Sadiq, and Al-Janabi, H., Shahad, Ak.K. (2003). A prediction study of a spark ignition supercharged hydrogen engine. *Energy Conversion and Management,* 44(20), 3143-3150. https://doi.org/10.1016/S0196-8904(03)00127-4 .

Azadi, M., and Parast, M.S.A., (2022) Data analysis of high-cycle fatigue testing on piston aluminum-silicon alloys under various conditions: Wear, lubrication, corrosion, nano-particles, heat-treating, and stress. *Data in Brief,* 41, 107984. https://doi.org/10.1016/j.dib.2022.107984 .

Cerit, M., (2011). Thermo mechanical analysis of a partially ceramic coated piston used in an SI engine. *Surface and Coatings Technology,* 205(11), 3499-3505. https://doi.org/10.1016/j.surfcoat.2010.12.019 .

Cerit, M., Coban, M., (2014). Temperature and thermal stress analyses of a ceramic-coated aluminum alloy piston used in a diesel engine. *International Journal of Thermal Sciences,* 77, 11-18. https://doi.org/10.1016/j.ijthermalsci.2013.10.009 .

Deulgaonkar, V.R., Ingolikar, N., Borkar, A., Ghute, S., and Awate, N., (2021). Failure analysis of diesel engine piston in transport utility vehicles. *Engineering Failure Analysis,* 120, 105008. https://doi.org/10.1016/j.engfailanal.2020.105008.

Dudareva, N.Y., Enikeev, R.D., and Ivanov, V.Y. (2017). Thermal protection of internal combustion engines pistons. *Procedia Engineering,* 206, 1382-1387. https://doi.org/10.1016/j.proeng.2017.10.649 .

Durat, M., Kapsiz, M., Nart, E., Ficici, F., and Parlak, A. (2012). The effects of coating materials in spark ignition engine design. *Materials & Design,* 36, 540-545. https://doi.org/10.1016/j.matdes.2011.11.053 .

Gai, S., Zhao, J., (2022). Simulation and experimental investigation on fatigue resistance of the forged steel piston in high-duty engine. *Journal of Materials Engineering and Performance.* https://doi.org/10.1007/s11665-022-07316-z .

Garbinčius, G., Bartulis, V., Pečeliūnas, R., & Pukalskas, S., (2005). The influence of coolant scale deposit inside the internal combustion

engine on the piston and cylinder deformations. *Transport,* 20(3), 123-128. https://doi.org/10.3846/16484142.2005.9638008 .

Ikonnikova, S.A., Scanlon, B.R., and Berdysheva S.A. (2023). A global energy system perspective on hydrogen Trade: A framework for the market color and the size analysis. *Applied Energy,* 330, 120267. https://doi.org/10.1016/j.apenergy.2022.120267 .

Ismail, I., Abdelrazek, E., Ismail, M., and Emara, A., (2020). An Investigation Study of the Thermomechanical Loading on the Piston of a Diesel Engine with Design Improvements. *SAE,* 2020-01-5098. https://doi.org/10.4271/2020-01-5098 .

Kakaee, A., Gharloghi, J., Foroughifar, A., Khanlari, A. (2015). Thermo-mechanical analysis of an SI engine piston using different boundary condition treatments. *J. Cent. South Univ,*. 22, 3817–3829. https://doi.org/10.1007/s11771-015-2926-7 .

Koutsakis, G., Begley, M.R., Hutchinson, J.W., and J.B. Ghandhi, (2022). Fracture-based transient thermo-mechanical analysis of reciprocating engine thermal barrier coatings. *Engineering Fracture Mechanics,* 270, 108568. https://doi.org/10.1016/j.engfracmech.2022.108568 .

Kowalski, S., Cie´slikowski, B., Barta, D., Dižo, J., Dittrich, (2023). A. Analysis of the Operational Wear of the Combustion Engine Piston Pin. *Lubricants,* 11, 100. https://doi.org/10.3390/lubricants11030100 .

Pratiksha, L., Bewoor, A., Kumar, R., Said, N.M., and Sharifpur, M. (2022). Benchmark using multi criteria decision making (MCDM) technique to optimally select piston material. *Engineering Analysis with Boundary Elements,* 142, 52-60. https://doi.org/10.1016/j.enganabound.2022.05.025 .

Mancaruso, E., and Sequino, L., (2019). Measurements and modeling of piston temperature in a research compression ignition engine during transient conditions. *Results in Engineering,* 2, 100007. https://doi.org/10.1016/j.rineng.2019.100007 .

Najafi, M., Dastani, H., Abedini, M., and Pirani, S. (2019). Stress Analysis and Fatigue Life Assessment of a Piston in an Upgraded Engine. *Journal of Failure Analysis and Prevention,* 19, 402-411. https://doi.org/10.1007/s11668-019-00583-4

Nguyen-Thi, T. X., and Bui T.M.T., (2023). Effects of Injection Strategies on Mixture Formation and Combustion in a Spark-Ignition Engine Fueled with Syngas-Biogas-Hydrogen. *International Journal of Renewable Energy Development,* 12(1), 118-128. https://doi.org/10.14710/ijred.2023.49368 .

Pingkuo, L., and Xue., H. (2022). Comparative analysis on similarities and differences of hydrogen energy development in the World's top 4 largest economies: A novel framework. *International Journal of Hydrogen Energy,* 47(16), 9485-9503. https://doi.org/10.1016/j.ijhydene.2022.01.038 .

Ramegouda, R., and Joseph, A.A., (2021). Effect of Compression Ratio on Performance and Emission Characteristics of Dual Spark Plug Ignition Engine Fueled With n-Butanol as Additive Fuel. *International Journal of Renewable Energy Development,* 10(1), 37-45. https://doi.org/10.14710/ijred.2021.32364 .

Satyanarayana, K., Rao, P.V.J.M., Kumar, I.N.N., Prasad, V.V.S., and Rao, T.V.H. (2018). Some studies on stress analysis of a sundry variable compression ratio diesel engine piston. *Materials Today: Proceedings* 5, no. 9, 18251-18259. https://doi.org/10.1016/j.matpr.2018.06.162 .

Scovell, M.D., (2022). Explaining hydrogen energy technology acceptance: A critical review. *International Journal of Hydrogen Energy,* 47(19), 10441-10459. https://doi.org/10.1016/j.ijhydene.2022.01.099 .

Tan, L.G., Li, G.L., Tao, C., and P.F. Feng, (2022). Study on fatigue life prediction of thermal barrier coatings for high-power engine pistons. *Engineering Failure Analysis,* 138, 106335. https://doi.org/10.1016/j.engfailanal.2022.106335 .

Venkatachalam, G., and Kumaravel A. (2019). Experimental Investigations on the Failure of Diesel Engine Piston. *Materials Today: Proceedings,* 16, 1196-1203. https://doi.org/10.1016/j.matpr.2019.05.214 .

Vichos, E., Sifakis, N., and Tsoutsos, T. (2022). Challenges of integrating hydrogen energy storage systems into nearly zero-energy ports. *Energy,* 241, 122878. https://doi.org/10.1016/j.energy.2021.122878 .

Zhenwei, W., Jianping, W., Changwen, H., Jiabing, S., Baoguo, X., and Xingquan, Z. (2022). Cracking failure analysis of steel piston forging die. *Engineering Failure Analysis,* 138, 106291. https://doi.org/10.1016/j.engfailanal.2022.106291 .

Zhou, Y., Li, X., Ding, S., Zhao, S., Zhu, K., Shao, L., Du, F., Wang, G., and Xu, Z. (2022). Technologies and studies of gas exchange in two-stroke aviation piston engine: A review. *Chinese Journal of Aeronautics,* 2022. https://doi.org/10.1016/j.cja.2022.08.012 .